OPEN

PRS GLOBAL OPEN

ORIGINAL ARTICLE

Pediatric/Craniofacial

Three-dimensional Coordinate System for Hemifacial Microsomia

Dai Ariizumi, DDS*
Teruo Sakamoto, DDS, PhD*
Takenobu Ishii, DDS, PhD*
Kenji Sueishi, DDS, PhD*
Yasushi Nishii, DDS, PhD*
Yoshiaki Sakamoto, MD†
Hisao Ogata, MD†

Background: Hemifacial microsomia (HFM) is a congenital disorder characterized by facial asymmetry, but no midline reference has been established for evaluating facial morphology in patients with HFM. The purpose of this study was to develop a 3-dimensional coordinate system unaffected by the deformity of the external acoustic aperture or orbital circumference and to quantitatively evaluate craniofacial morphology in such patients.

Methods: We quantitatively evaluated craniofacial morphology using 3-dimensional measurements with the skull base as a reference. Using computed tomography data from 15 patients with HFM and 15 controls, a coordinate system was created for each patient, and left–right differences between measurement points were compared.

Results: When mandibular deformity was severe, the deformity of the posterior part of the palatine bone and lateral part of the orbit increased, but this trend was not evident for other measurement points. Thus, craniofacial deformity in HFM was not always related to mandibular deformity. Moreover, no difference was evident in the position of the hypoglossal canal between controls and patients with HFM.

Conclusions: Quantitative assessments are possible using the coordinate system devised in this study, irrespective of the severity of HFM. The degree of mandibular deformity detailed in the Pruzansky classification was associated with the superoinferior deformity of the posterior part of the palatine bone and anteroposterior deformity of the lateral part of the orbit. *(Plast Reconstr Surg Glob Open 2020;8:e2761; doi: 10.1097/GOX.0000000000002761; Published online 29 April 2020.)*

INTRODUCTION

The Pruzansky[1] classification is widely used for the morphologic classification of hemifacial microsomia (HFM) and categorizes the condition into types I–III according to the severity of mandibular malformation. Various reports have described the treatment of this condition, but few provide treatment-related morphologic analyses or assess posttreatment changes. Accurately determining the median sagittal plane in patients with HFM with the conventional 2-dimensional method used to determine the midline in orthodontic patients is often difficult, producing distortion in the face.[2] Matsuno et al,[3] in a computed tomographic (CT) study of one patient with HFM and another with cleft lip and palate, observed that assessment using 3-dimensional (3D) coordinates is useful in the morphologic recognition of patients with craniomaxillofacial deformities. However, in a study of 3D morphologic measurements in patients with HFM, Shibazaki et al[4] stated that type III deformity is quite different to types I and II. Additionally, HFM also affects the orbital circumference, and unilateral aural atresia is present in half of these patients[5]; therefore, assessment methods that attempt to use the external acoustic aperture and orbital circumference as reference planes for all 3 types of HFM encounter difficulty.

Morphologic analyses of HFM require a more universal and accurate assessment method. In this study, we assessed the craniofacial morphology of HFM using a coordinate system unaffected by the deformity of the external acoustic aperture or orbital circumference.

METHODS

Study Design

To address the research purpose, we designed and implemented a cross-sectional study. The study population

*From the *Department of Orthodontics, Tokyo Dental College, Chiba, Japan; and †Department of Plastic and Reconstructive Surgery, Keio University School of Medicine, Tokyo, Japan.*

Received for publication December 18, 2019; accepted February 10, 2020.

DOI: 10.1097/GOX.0000000000002761

Disclosure: *The authors have no financial interest to declare in relation to the content of this article.*

was composed of all patients presenting to the Department of Plastic and Reconstructive Surgery at Keio University Hospital, Tokyo, Japan, for the evaluation and management of HFM. To be included in the study sample, the patients had to meet the following inclusion criteria: (1) unilateral, (2) no metal prosthesis, (3) no Goldenhar syndrome, and (4) no cleft palate and lip.

Patients with head contusions excluding patients with fractures without anomalies or skeletal problems (asymmetry and anteroposterior) examined in the same department formed a control group. Fifteen HFM patients were selected and divided into 3 groups according to the Pruzansky[1] classification by attending doctor of Keio University Hospital: type I (mandibular hypoplasia is minimal or slight), type II (the condyle and ramus are small and abnormally shaped), and type III (the ramus is reduced to a thin lamina of bone, or it is completely absent) (Fig. 1).

CT was performed using LightSpeed 16 (GE Healthcare, Milwaukee, Wisc.), BrightSpeed S (GE Healthcare), and Discovery CT750 HD (GE Healthcare) CT scanners at the following settings: 120 kV; 70–300 mA; slice thickness, 0.625 mm; and field of view, 25 cm.

CT data for each patient minus names and identification numbers were saved in DICOM (digital imaging and communications in medicine) format at Keio University Hospital, then converted to stereolithography data using 3D structural analysis software (TRI/3D-BON version 9.0; RATOC System Engineering, Tokyo, Japan) at Tokyo Dental College. A coordinate system centered on the hypophyseal fossa was prepared for each patient using 3D measurement point data processing software (Imageware version 13.2; Siemens AG, Munich, Germany), and the 3D coordinates of arbitrary points were measured.

This study was conducted with approval for the use of these data from the ethics committees at Keio University Hospital (approval number: 20120137) and Tokyo Dental College (approval number: 285).

Development of the Coordinate System

The dimensions of the sella turcica of each patient were calculated using the width of the hypophyseal fossa, and a cylinder was prepared using the maximum contact area with the middle clinoid process, hypophyseal fossa, and posterior clinoid process. The center point of the central axis of this cylinder was taken as the origin of the coordinate system. The left–right direction was defined as the *x* axis, the anteroposterior direction as the *y* axis, and the superoinferior direction as the *z* axis, and a coordinate system was established using the following conditions (Figs. 2–6):

- *x* axis: orthogonal to the *y* and *z* axes, with the left side taken as the positive direction.
- *y* axis: parallel to the line connecting the midpoint of the most posterior points of the left and right occipital condyles and the most posterior point of the foramen cecum, with the posterior direction taken as the positive direction.
- *z* axis: parallel to the straight line connecting the origin and posterior point of the junction of the inferior border of the vomer and nasal crest of the horizontal plate of the palatine bone, and orthogonal to the line connecting the origin and foramen cecum. The superior direction was taken as the positive direction.

Measurements

Thirty points were measured on the 17 areas listed in Table 1, and the 3D coordinates of each point were measured.

In the control group, the reference plane indices conventionally used in 3D analysis [anterior nasal spine (ANS), nasion (N), crista galli (Cr), basion (Ba), and porion (Po)][6–13] were also measured.

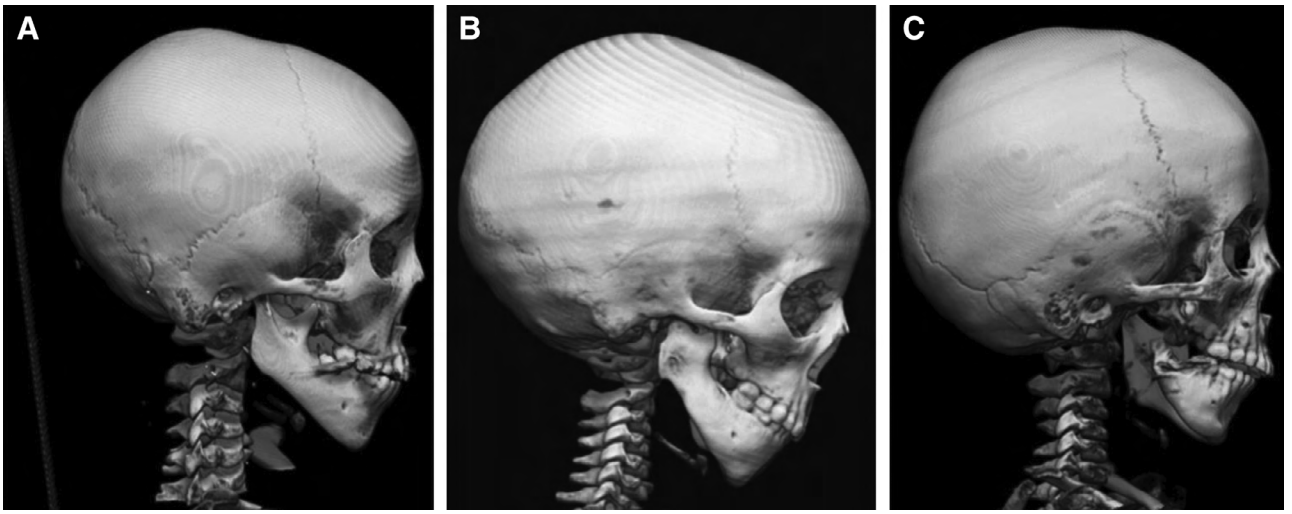

Fig. 1. The affected side in patients with hemifacial microsomia. A, Type I: the skeleton shows a normal shape and hypoplasia is slight. B, Type II: the condyle is flattened, and the coronoid process and ramus are small. The external acoustic aperture is absent on the affected side in this patient. C, Type III: the complete absence of the ramus and mandibular fossa.

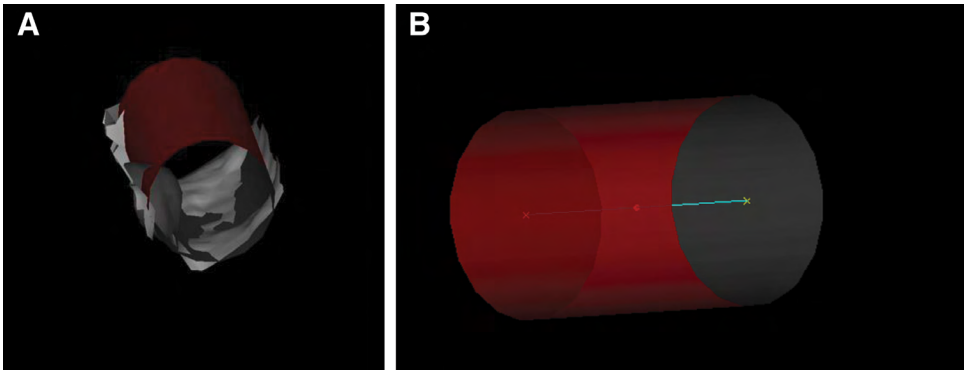

Fig. 2. Creating the origin of the coordinate system. A, The cylinder fits in the hypophyseal fossa. B, The center point of the central axis of the cylinder is taken as the origin for the coordinate system.

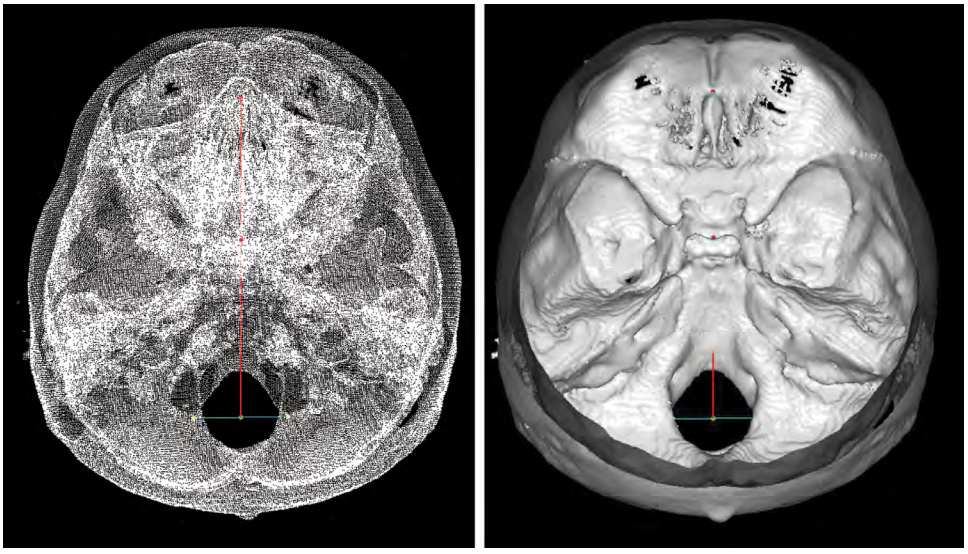

Fig. 3. *Y* axis indicator: line connecting the center point of the left and right occipital condyles and the foramen cecum.

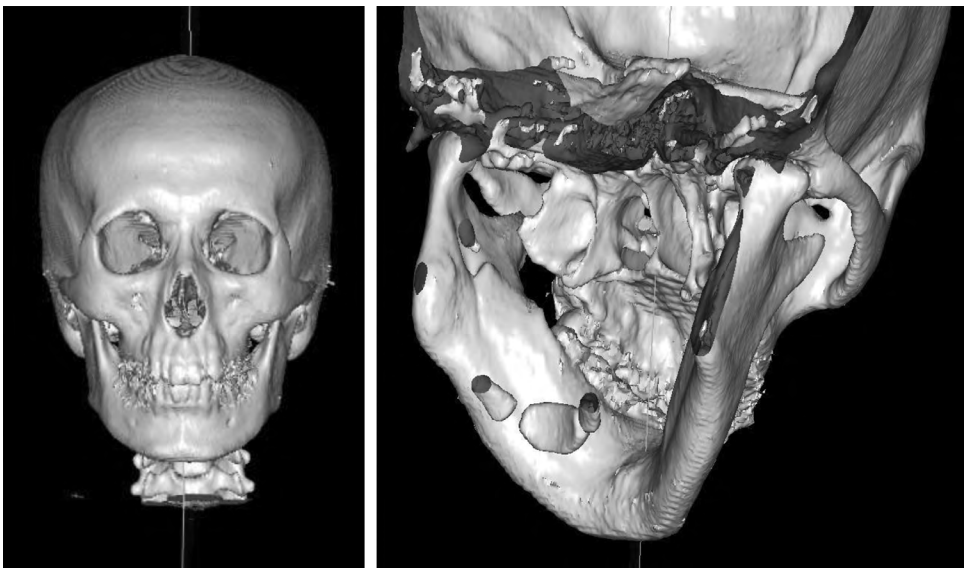

Fig. 4. *Z* axis indicator: origin and posterior border of vomer–nasal crest junction.

Statistical Analysis

Considering the individual differences between subjects, each coordinate value of the 3D coordinate data obtained for each patient was adjusted by a multiplying factor, so that the *y* coordinate of the foramen cecum was −50 (mm). Left–right differences (calculated with absolute differences for the *x* and *y* coordinates) were then calculated, with values for the left and right sides measured as *x*, *y*, and *z* coordinate values, as follows:

HFM group: (unaffected side) − (affected side); and
control group: (left side) − (right side).

A multiple comparison test of values obtained for the left–right differences between each coordinate was then performed using Dunnett's test. For left–right differences in *z* coordinates, there were areas for which positive and negative coordinate values did not correspond to the left and right, and calculations were made without using absolute values. In the control group, the *t* test was conducted for *z* coordinates of the left and right Po, and Tukey's test was conducted for *x* coordinates of the ANS, N, Cr, and Ba. *P* value <0.05 was considered statistically significant.

With regard to single measurement points [incisive foramen, ANS, posterior nasal spine (PNS), foramen cecum, N, and Cr], the value assessed was the mean value of the *x* coordinate.

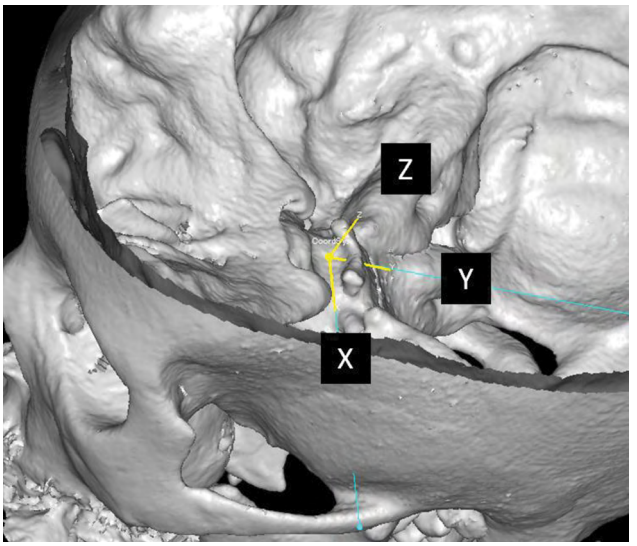

Fig. 5. The coordinate origin and coordinate axis direction of the coordinate system of this study created in the right-handed system (world coordinate system).

RESULTS

Fifteen patients had HFM (type I, 5 patients; type II, 5 patients; type III, 5 patients; mean age, 12.9 years; range, 8–17 years). The control group had 15 patients (mean age, 13.1 years; range, 7–16 years).

In the control group, little difference was evident in the reference plane indices (ANS, N, Cr, Ba, and Po) conventionally used in 3D analysis (mean *x* coordinate values of ANS, 0.41 mm; N, 0.12 mm; Cr, 0.40 mm; Ba, 0.34 mm; mean *z* coordinate value of the Po, left side −14.25 mm and right side −14.22 mm).

From the 30 measurement points in the 30 patients used in this study, 2,700 coordinate values were obtained. Tables 2–4 show the mean left–right differences calculated and the mean *x* coordinate values of single measurement points.

Areas significantly different to the control group arranged by HFM type comprised (Figs. 7–15):

Type I: no areas showed significant differences.
Type II: greater palatine foramen *z* coordinate ($P < 0.05$); frontozygomatic suture *y* coordinate ($P < 0.05$); foramen rotundum *x* coordinate ($P < 0.05$); and foramen ovale *z* coordinate ($P < 0.05$).

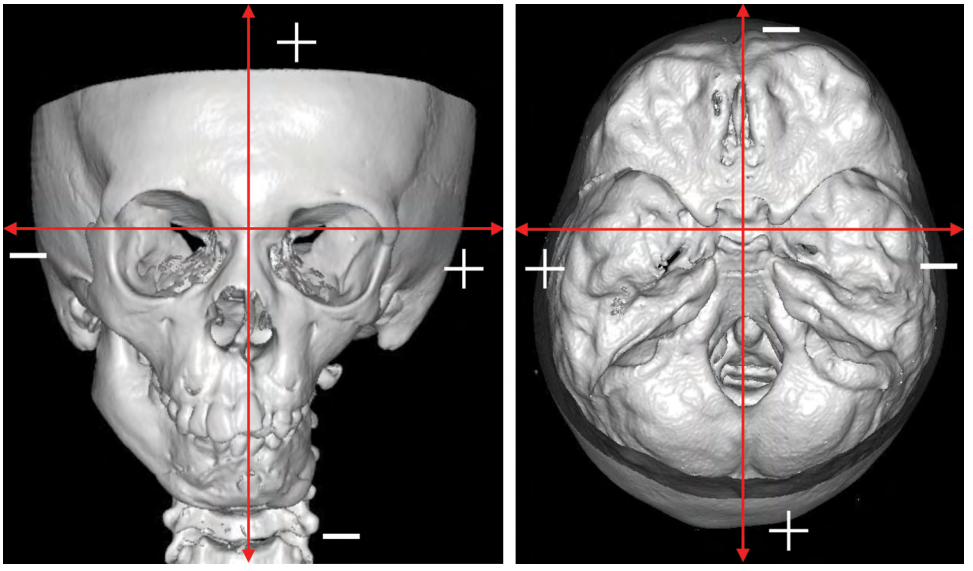

Fig. 6. The *x*, *y*, and *z* axes of the coordinate system are shown. Positive directions on the axes were taken to be the left on the *x* axis, posterior on the *y* axis, and superior on the *z* axis.

Table 1. Measurement Points and Definitions Used in This Study

Landmark	Abbreviation	Definition
Incisive foramen	Inf	Most posterior point of incisive foramen
Anterior nasal spine	ANS	Point of union of left and right anterior nasal spine
Posterior nasal spine	PNS	Apex of posterior nasal spine
Foramen cecum	Fc	Posterior point of the foramen cecum
Greater palatine foramen	Gpf	Most posterior point of greater palatine foramen
Infraorbital foramen	Ior	Most superior point of infraorbital foramen
Nasolacrimal duct	Nlc	Most anterior point of nasolacrimal duct
Frontozygomatic suture	Fzs	Most anterior point of frontozygomatic suture
Superior orbital fissure	Sof	Most lateral point of superior orbital fissure
Medial border of optic canal	Opi	Most medial point of optic canal opening
Superior border of optic canal	Opt	Most superior point of optic canal opening
Foramen rotundum	Fro	Most superior point of foramen rotundum
Foramen ovale	Fov	Most anterior point of foramen ovale
Internal acoustic opening	Ina	Most superior point of internal acoustic opening
Hypoglossal canal	Hyp	Most anterior point of the intracranial opening of the hypoglossal canal
Sp point	Sp	Most lateral point of lesser wing of sphenoid bone
Sig point	Sig	Most lateral point of groove for sigmoid sinus
Nasion	N	Midpoint of frontonasal suture
Crista galli	Cr	Apex of ethmoid crista galli
Basion	Ba	Most posterior point of foramen magnum
Porion	Po	Superior margin of external acoustic aperture

Table 2. Mean Value (Millimeter) of Left–Right Differences in *X* Coordinates

Measurement Points	Type I	Type II	Type III	Control
Inf	−0.88	1.28	−1.42	0.48
ANS	−0.83	0.15	−1.21	0.41
PNS	−0.26	0.54	0.14	−0.04
Fc	−0.71	0.33	0.17	0.48
Gpf	0.42	−0.99	−1.66	0.51
Ior	−1.51	1.18	−1.38	0.44
Nlc	−1.04	−0.87	−0.87	0.67
Fzs	−1.55	−0.54	−0.90	0.26
Sof	−1.96	−1.90	−2.32*	−0.04
Opi	−1.48	0.04	−0.50	−0.02
Opt	−1.48	0.15	−0.50	0.25
Fro	−0.20	−1.72*	−0.42	0.81
Fov	−1.24	−1.38	0.75	0.32
Ina	−0.75	0.40	1.02	0.23
Hyp	−0.69	−0.31	−0.29	0.82
Sp	−4.26	−2.05	−2.59	−0.63
Sig	−0.14	−0.21	2.32	1.21

Mean measured values are shown because Inf, ANS, PNS, and Fc are single points. Colored portion indicates measurement point for which the mean value for all groups was −1.1 to 1.1 mm.
*$P < 0.05$ compared with control group.
Fc, foramen cecum; Fov, foramen ovale; Fro, foramen rotundum; Fzs, frontozygomatic suture; Gpf, greater palatine foramen; Hyp, hypoglossal canal; Ina, internal acoustic opening; Inf, incisive foramen; Ior, infraorbital foramen; Nlc, nasolacrimal duct; Opi, medial border of optic canal; Opt, superior border of optic canal; Sig, Sig point; Sof, superior orbital fissure; Sp, Sp point.

Table 3. Mean Value (Millimeter) of Left–Right Differences in *Y* Coordinates

Measurement points	Type I	Type II	Type III	Control
Gpf	−1.24	0.44	0.75	−0.62
Ior	−0.44	0.20	0.66	−0.20
Nlc	−0.48	0.62	−0.35	−0.71
Fzs	−0.03	3.50*	4.68†	0.19
Sof	−0.41	0.59	0.47	0.06
Opi	−0.87	0.27	−0.32	−0.21
Opt	−0.16	0.72	0.04	−0.06
Fro	0.22	1.66	1.61	0.24
Fov	0.03	−1.75	0.38	−0.81
Ina	1.43	−0.91	2.40*	−1.10
Hyp	0.46	0.24	0.08	−1.08
Sp	−0.01	2.71	1.28	0.49
Sig	1.57	−0.31	3.70	−0.51

Colored portion indicates measurement point for which the mean value for all groups was −1.1 to 1.1 mm.
*$P < 0.05$ compared with control group.
†$P < 0.01$ compared with control group.
Fov, foramen ovale; Fro, foramen rotundum; Fzs, frontozygomatic suture; Gpf, greater palatine foramen; Hyp, hypoglossal canal; Ina, internal acoustic opening; Ior, infraorbital foramen; Nlc, nasolacrimal duct; Opi, medial border of optic canal; Opt, superior border of optic canal; Sig, Sig point; Sof, superior orbital fissure; Sp, Sp point.

Type III: greater palatine foramen z coordinate ($P < 0.01$); infraorbital foramen z coordinate ($P < 0.01$); nasolacrimal duct z coordinate ($P < 0.01$); frontozygomatic suture y coordinate ($P < 0.01$); superior orbital fissure x coordinate ($P < 0.05$); foramen rotundum z coordinate ($P < 0.05$); and internal acoustic opening y coordinate ($P < 0.05$).

The greater palatine foramen z coordinate and frontozygomatic suture y coordinate were related to the Pruzansky[1] classification; when mandibular deformity was severe, the deformity of the posterior part of the palatine bone and lateral part of the orbit was also severe. A significant difference was evident in the z coordinate of nasolacrimal duct (a measurement item on the maxilla) and in the infraorbital z coordinate in type III HFM, and their left–right differences yielded a negative value. The measurement point on the affected side was located superiorly. A significant difference in the x coordinate of the superior orbital fissure was seen in type III HFM only, but the left–right difference yielded a negative value in types I–III HFM, and the affected side tended to be located more laterally than the unaffected side. For the foramen rotundum, a significant difference in the x coordinate was evident in type II HFM, and the affected side was located laterally. A significant difference was evident in the z coordinate in type III HFM, and the affected side was located superiorly. Likewise, in type II HFM, although no significant difference was found in the z coordinate, the affected side tended to be located superiorly. For the z coordinate of the foramen ovale, a significant difference was also only evident in type II HFM and, similarly to the x coordinate of the foramen rotundum, was not associated with the degree of mandibular deformity. A significant difference

Table 4. Mean Value (Millimeter) of Left–Right Differences in *Z* Coordinates

Measurement Points	Type I	Type II	Type III	Control
Gpf	−0.73	−4.84*	−5.85†	−0.47
Ior	−0.13	−1.63	−5.22†	0.46
Nlc	−0.18	−0.32	−3.56†	−0.59
Fzs	1.43	0.31	−2.36	−0.20
Sof	0.87	0.47	−1.60	−0.64
Opi	0.10	0.27	−0.44	0.16
Opt	0.23	0.14	−1.11	−0.14
Fro	0.08	−1.26	−2.45*	0.45
Fov	0.55	−3.49*	−2.65	−0.22
Ina	0.43	0.84	0.69	0.37
Hyp	0.18	−0.70	0.88	−0.48
Sp	1.47	1.60	−1.28	−0.99
Sig	3.06	2.54	3.61	−0.61

Colored portion indicates measurement point for which the mean value for all groups was −1.1 to 1.1 mm.
*$P < 0.05$ compared with control group.
**$P < 0.01$ compared with control group.
Fov, foramen ovale; Fro, foramen rotundum; Fzs, frontozygomatic suture; Gpf, greater palatine foramen; Hyp, hypoglossal canal; Ina, internal acoustic opening; Ior, infraorbital foramen; Nlc, nasolacrimal duct; Opi, medial border of optic canal; Opt, superior border of optic canal; Sig, Sig point; Sof, superior orbital fissure; Sp, Sp point.

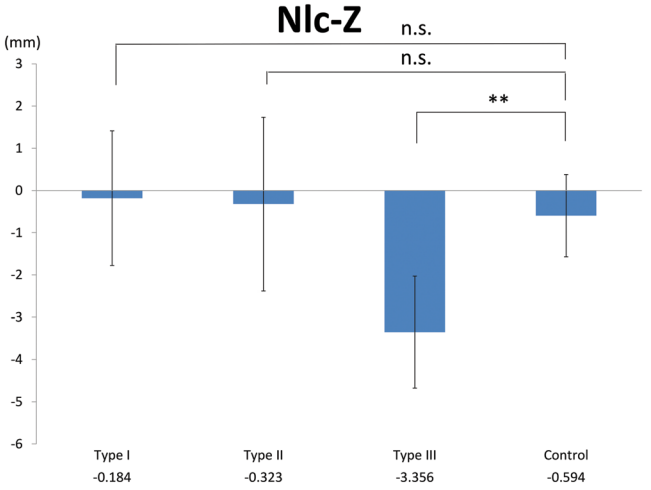

Fig. 9. Nlc-*z*: *z* coordinates of the nasolacrimal duct. n.s. not significant. **$P < 0.01$ compared with control group.

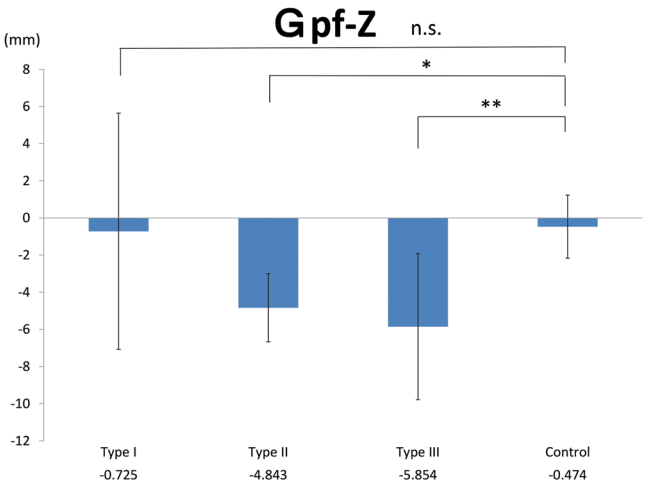

Fig. 7. Areas significantly different to the control group. Gpf-*z*: *z* coordinates of the greater palatine foramen. n.s., not significant. *$P < 0.05$ compared with control group. **$P < 0.01$ compared with control group.

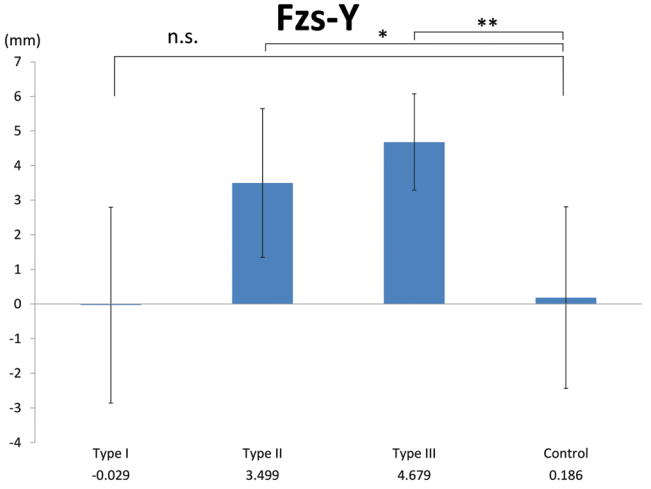

Fig. 10. Fzs-*y*: *y* coordinates of the frontozygomatic suture.

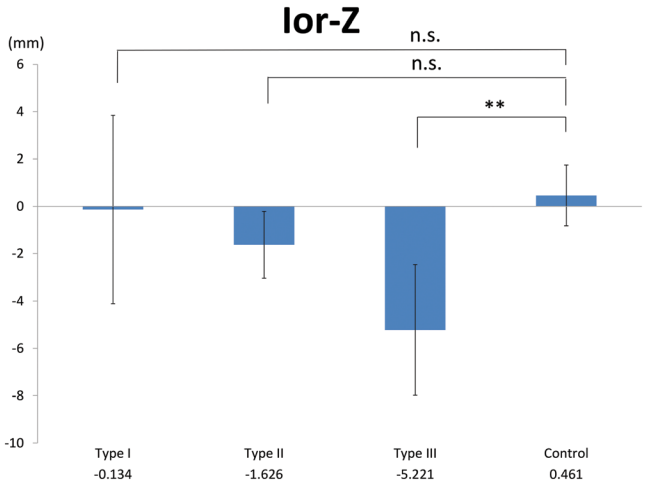

Fig. 8. Ior-*z*: *z* coordinates of the infraorbital foramen. n.s. not significant. **$P < 0.01$ compared with control group.

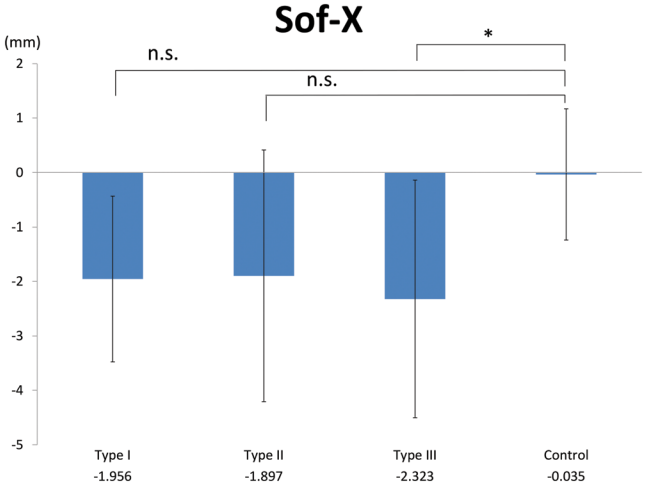

Fig. 11. Sof-*x*: *x* coordinates of the superior orbital fissure. n.s. not significant. *$P < 0.05$ compared with control group.

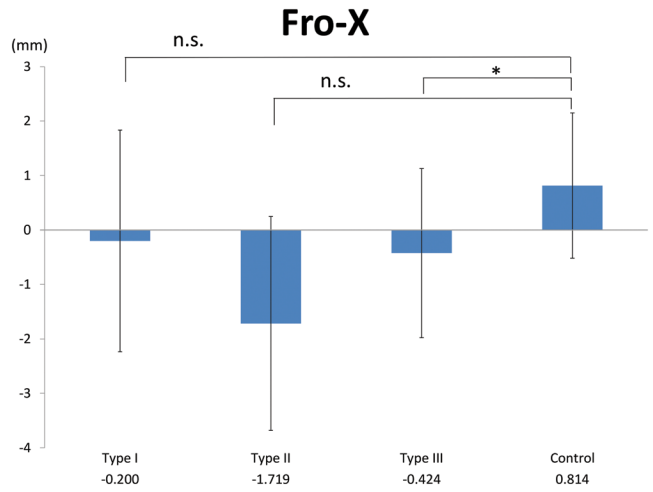

Fig. 12. Fro-*x*: *x* coordinates of the foramen rotundum. n.s. not significant. *$P < 0.05$ compared with control group.

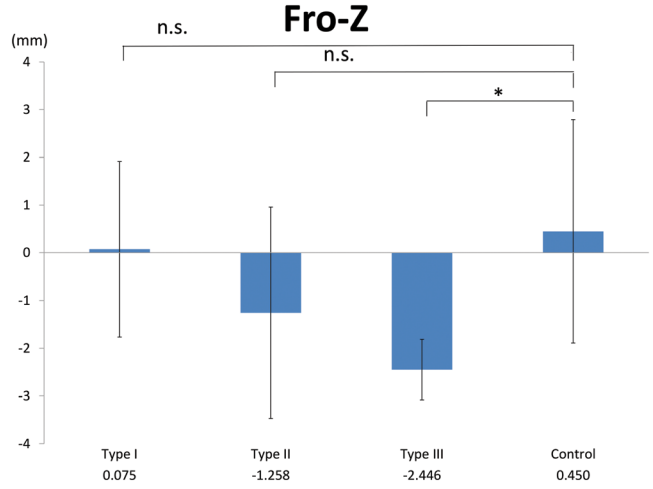

Fig. 13. Fro-*z*: *z* coordinates of the foramen rotundum. n.s. not significant. *$P < 0.05$ compared with control group.

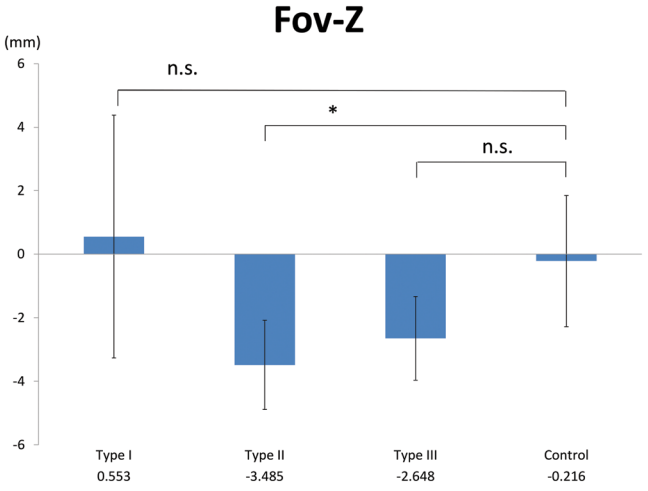

Fig. 14. Fov-*z*: *z* coordinates of the foramen ovale. n.s. not significant. *$P < 0.05$ compared with control group.

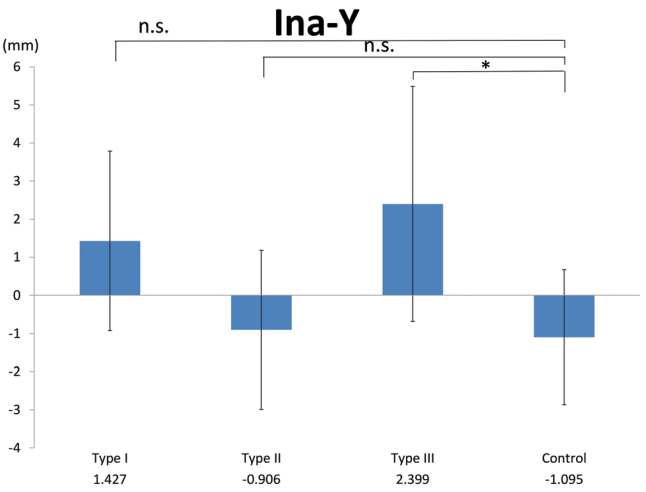

Fig. 15. Ina-*y*: *y* coordinates of the internal acoustic opening. n.s. not significant. *$P < 0.05$ compared with control group.

was evident in the *y* coordinate of the internal acoustic opening in type III HFM, and the affected side was located anteriorly.

Among the areas for which a significant difference was not evident, the coordinate values of mean x coordinate value of posterior nasal spine (PNS-x), mean x coordinate value of foramen cecum (FC-x), mean y coordinate value of infraorbital foramen (Ior-y), mean x coordinate value and mean y coordinate value of nasolacrimal duct (Nlc-xy), mean y coordinate value of superior orbital fissure (Sof-y), mean y coordinate value and mean z coordinate value of medial border of optic canal (Opi-yz), mean y coordinate value of superior border of optic canal (Opt-y), mean x coordinate value and mean y coordinate value of inter acoustic opening (Ina-xy), and mean x coordinate value, mean y coordinate value and mean z coordinate value of hypoglossal canal (Hyp-xyz) displayed particularly small differences, and the mean values for their left–right differences were in the range of −1.1 to 1.1 mm in all groups. We considered that little deformity was evident in these areas.

DISCUSSION

Coordinate System

The center of the hypophyseal fossa was used as the origin of the coordinate system in this study. The sella turcica is a point appropriate for the assessment of symmetry because it is located at the center of the base of the skull; moreover, it has been used as an indicator of the median sagittal plane in many 3D measurement studies.[7,9,11,13] In a study on the consistency and precision of anatomical landmarks using 3D cone beam CT, Schlicher et al[14] stated that the sella turcica is the point with the highest reproducibility. In a preliminary experiment, we found that there was <1 mm difference in the *x* coordinate values between the center point of the cylinder and the line connecting the foramen cecum and center point of the left and right occipital condyles between the control and HFM groups.

The cranial base deformity was considered insufficient to change the width of the hypophyseal fossa, and the use of the hypophyseal fossa as the origin in this coordinate system was appropriate.

In a preliminary experiment, the central axis of a cylinder occupying the hypophyseal fossa was used as the *x* axis, but this axis was clearly not horizontal in some subjects in both the HFM and control groups. The vomer, in which deformity never occurs in HFM, was therefore used as a reference in this experiment. Hlaing et al[15] investigated the morphology of the sella turcica, dividing it into 4 categories based on the position of the indentation of the hypophyseal fossa. The complexity of the shape of the hypophyseal fossa is thought to manifest as an inclination of the cylinder. In determining the coordinate axis of patients with left–right asymmetry, an axis defined using bilateral landmarks that exist in the region of the deformity is inappropriate. In this study, therefore, the *x* axis was established as an axis perpendicular to the *y* and *z* axes.

In determining the *y* axis, it was necessary to use a landmark located in the center of the body. The cervical spine is thought to be located at the center of the body irrespective of facial symmetry, and Maeda et al[9] used the apex of the dens to determine the midline. However, the dens may deviate from the center as a result of head position during CT and were inappropriate for this study. The center of the foramen magnum relative to the dens has also been used,[12] but in measurements using CT images, landmarks located on a curve are reportedly susceptible to measurement error,[14] and the posterior border of the occipital condyle, which can be viewed as a single point more easily than the lateral border of the foramen magnum, was thought to offer better reproducibility. The neural foramen is clearly recognizable on CT, and for this reason, the foramen cecum rather than the Cr was used as the anterior reference point. As the developmental abnormalities of HFM originate in the first and second branchial arches[16] and there is little effect from muscle force on the base of the skull where the neural canal and foramen cecum exist,[17] displacement of the neural canal in the region of the ethmoid and frontal bones is unlikely; therefore, the foramen cecum constituted a valid midline reference point.

The control group showed little difference between midline reference points using conventional areas (ANS, N, Cr, and Ba) and the horizontal reference point (left and right Po), and the assessment using the coordinate system developed in this study was judged comparable to that obtained using conventional methods in individuals without congenital abnormalities.

Study Results

Compared with the control group, significant differences were evident in 7 areas in type III HFM and 4 areas in type II, but no areas in type I. This suggests that the craniofacial morphology of type I exhibits little deformity, and that deformity is more extensive in type III than in type II. The *z* coordinate of the greater palatine foramen and the *y* coordinate of the frontozygomatic suture were associated with the Pruzansky[1] classification (type II, $P < 0.05$; type III, $P < 0.01$), and when mandibular deformity was severe, large superoinferior deformity of the posterior part of the palatine bone and anteroposterior deformity of the lateral part of the orbit also occurred. Although a significant difference was observed in the *z* coordinate of the greater palatine foramen, because the *x* coordinate of the PNS was located very near the center, deformity of the palatine bone on the affected side may occur as if it has rotated centered on the midline of the palate.

Tendencies for the superior displacement of the nasolacrimal duct, infraorbital foramen, foramen rotundum, and foramen ovale were evident on the affected side. The maxilla and greater wing of the sphenoid bone were displaced superiorly or deformed on the affected side. The superior orbital fissure showed a tendency for lateral displacement in all HFM types. Although the sphenoid bone does not originate from the first and second branchial arches, the deformity was evident in patients with the sphenoid bone in the center of the base of the skull. This may result from contact with the maxilla, zygomatic bone, or temporal bone, which do originate from the first and second branchial arches. In HFM, developmental disorders are thought to occur in bone and soft tissue originating from the first and second branchial arches, but developmental disorders may also affect the formation of those or neighboring bones as a result of the action of muscles.

Craniofacial deformity in HFM is not uniform, and many variations exist.[4] Vargervik and Miller[18] investigated growth patterns in HFM; they stated that it is necessary to understand not only morphologic changes but also neuromuscular functions. In patients with HFM, unlike in symmetric individuals, clear left–right differences exist in the activity of the muscles of facial expression and mastication.[19] The differences in these muscles may make the variations in the deformities of HFM even more complex.

Kim et al[20] conducted morphologic measurements of dry skulls, observing that when there is deformity in the cranium, deformity probably also exists in the base of the skull. In this study, there was no significant difference between the craniums of type I patients and those of the control group, but it cannot be concluded that they were completely unaffected. The SD of the left–right difference in the vertical position of the greater palatine and infraorbital foramina was larger than in the control group, suggesting some level of deformity even in type I HFM.

However, of those areas not significantly different to the control group, little left–right difference was evident in the hypoglossal canal, particularly among patients with HFM, and this structure may represent a useful reference for 3D analysis.

CONCLUSIONS

In this study, we developed a coordinate system centered on the hypophyseal fossa to quantitatively assess craniofacial deformity in patients with HFM. Assessments made using this coordinate system were unaffected by facial deformity and can be used irrespective of the Pruzansky[1] classification. Hence, it was possible to quantify the morphologic analysis of patients with craniofacial asymmetry.

The degree of craniofacial deformity in HFM is not always related to the degree of mandibular deformity detailed in the Pruzansky[1] classification. There are various aspects of craniofacial deformity in HFM, but generally type I has a small range of deformity, whereas deformity is more extensive in type III than in type II HFM. Additionally, the superoinferior deformity of the posterior part of the palatine bone and anteroposterior deformity of the lateral part of the orbit are particularly associated with mandibular deformity.

Dai Ariizumi, DDS
Department of Orthodontics
Tokyo Dental College
1-2-2, Masago, Mihama-ku
Chiba, Japan 261-8502
E-mail: ariizumidai@tdc.ac.jp

ACKNOWLEDGMENTS

The authors thank the Departments of Plastic and Reconstructive Surgery and Radiology, Keio University, for the computed tomographic data used in this study. The authors also thank the Chief Research Engineer, Shigeru Okano, of the Oral Health Science Center, Tokyo Dental College, for his technical support in this study.

REFERENCES

1. Pruzansky S. Not all dwarfed mandibles are alike. *Birth Defects.* 1969;5:120.
2. Fushima K, Akimoto S, Takamoto K, et al. Morphological feature and incidence of TMJ disorders in mandibular lateral displacement cases. *Nihon Kyosei Shika Gakkai Zasshi.* 1989;48:322–328.
3. Matsuno I, Kawakami M, Yamamura M, et al. Three-dimensional morphological analysis for craniofacial deformity. *Nihon Kyosei Shika Gakkai Zasshi.* 1990;49:291–301.
4. Shibazaki R, Maki K, Nakano H, et al. Craniomaxillofacial morphology in growing Japanese hemifacial microsomia study using 3DCT [in Japanese]. *J Showa Univ Dent Soc.* 2002;22:113.
5. Reza R, Caroline DR, John BM, et al. Craniofacial, temporal bone, and audiologic abnormalities in the spectrum of hemifacial microsomia. *Arch Otolaryngol Head Neck Surg.* 2001;127:265.
6. Glat PM, Freund RM, Spector JA, et al. A classification of plagiocephaly utilizing a three-dimensional computer analysis of cranial base landmarks. *Ann Plast Surg.* 1996;36:469–474.
7. Kwon TG, Park HS, Ryoo HM, et al. A comparison of craniofacial morphology in patients with and without facial asymmetry–a three-dimensional analysis with computed tomography. *Int J Oral Maxillofac Surg.* 2006;35:43–48.
8. Park SH, Yu HS, Kim KD, et al. A proposal for a new analysis of craniofacial morphology by 3-dimensional computed tomography. *Am J Orthod Dentofacial Orthop.* 2006;129:600.e23–600.e34.
9. Maeda M, Katsumata A, Ariji Y, et al. 3D-CT evaluation of facial asymmetry in patients with maxillofacial deformities. *Oral Surg Oral Med Oral Pathol Oral Radiol Endod.* 2006;102:382–390.
10. Hwang HS, Hwang CH, Lee KH, et al. Maxillofacial 3-dimensional image analysis for the diagnosis of facial asymmetry. *Am J Orthod Dentofacial Orthop.* 2006;130:779–785.
11. Baek SH, Cho IS, Chang YI, et al. Skeletodental factors affecting chin point deviation in female patients with class III malocclusion and facial asymmetry: a three-dimensional analysis using computed tomography. *Oral Surg Oral Med Oral Pathol Oral Radiol Endod.* 2007;104:628–639.
12. Damstra J, Oosterkamp BC, Jansma J, et al. Combined 3-dimensional and mirror-image analysis for the diagnosis of asymmetry. *Am J Orthod Dentofacial Orthop.* 2011;140:886–894.
13. Zamora N, Llamas JM, Cibrián R, et al. A study on the reproducibility of cephalometric landmarks when undertaking a three-dimensional (3D) cephalometric analysis. *Med Oral Patol Oral Cir Bucal.* 2012;17:e678–e688.
14. Schlicher W, Nielsen I, Huang JC, et al. Consistency and precision of landmark identification in three-dimensional cone beam computed tomography scans. *Eur J Orthod.* 2012;34:263–275.
15. Hlaing Y, Allan JC, Kramer B. A reappraisal of the hypophysial region of the floor of the sella turcica. *Clin Anat.* 2012;25:324–329.
16. Kajii T, Kuroki Y, Niikawa N, et al. *New Atlas of Congenital Malformation Syndromes.* Tokyo, Japan: Nankodo; 1998.
17. Sekikawa M, Kanazawa E, Akai J, et al. An application of the coordinate measuring machine to three-dimensional measures of internal cranial base morphology. *Nichidai Koko Kagaku.* 1988;14:356–363.
18. Vargervik K, Miller AJ. Neuromuscular patterns in hemifacial microsomia. *Am J Orthod.* 1984;86:33–42.
19. Nishimura F, Sakamoto T, Sueishi K. Characteristics of facial muscle and activity of masticatory muscle in hemifacial microsomia [in Japanese]. *Shikwa Gakuho.* 2005;105:383.
20. Kim YH, Sato K, Mitani H, et al. Asymmetry of the sphenoid bone and its suitability as a reference for analyzing craniofacial asymmetry. *Am J Orthod Dentofacial Orthop.* 2003;124:656–662.